J Mater Sci: Mater Med (2008) 19:917–927
DOI 10.1007/s10856-007-0172-8

Dissolution and re-crystallization processes in multiphase silicon stabilized tricalcium phosphate

Loughlin Tuck · Roope Astala · Joel W. Reid · Michael Sayer · Malcolm J. Stott

Received: 26 July 2006 / Accepted: 20 February 2007 / Published online: 1 August 2007

Abstract Ultrasonically accelerated dissolution of multiphase silicon stabilized tricalcium phosphate powders in water or Earle's balanced salt solution transforms the powders into needle-like calcium deficient apatite crystals with the c-axis (001) oriented along the needle. Ion exchange with the solution occurs primarily in the first hours of immersion. The transformation is driven by an interaction between the crystal surface and adsorbed water leading to the growth of crystallites which have the most stable surface configuration. First principles calculations of the surface energies of various hydroxyapatite surfaces with and without adsorbed water shows that depending on the ion concentrations in the fluid that determine the chemical potential of tricalcium phosphate, either Ca-rich (010) or stoichiometric (001) layers are the dominant surfaces. The higher the chemical potential, the more elongated in the (001) direction the crystallites become to minimize the total surface energy. The loss of a calcium Ca^{2+} compensated by the addition of two H^+ is strongly favoured energetically on the (001) and Ca-rich (010) surfaces. A high concentration of excess Si at grain boundaries may be partly responsible for the rapid transformation of multiphase Si-TCP.

L. Tuck · R. Astala · M. Sayer (✉) · M. J. Stott
Department of Physics, Queen's University, Kingston, ON, Canada K7L 3N6
e-mail: sayerm@physics.queensu.ca

J. W. Reid
Millenium Biologix Corp., 785 Midpark Drive, Kingston, ON, Canada K7M 7G3

Introduction

The interfacial reactions between a biomaterial and an aqueous environment play an important role in influencing cellular activity on the material by affecting the composition of the extracellular environment and the material surface. Calcium phosphates are the most common materials used in bone substitute applications [1, 2] because of their chemical similarities to the inorganic component of bone. The solubility of calcium phosphate compounds with different Ca/P ratios in an aqueous solution at ambient temperature varies widely. The reactions of calcium phosphates with water and biological media are of great interest when these materials are used in biomaterial applications.

Trace elements such as silicon are recognized as having important effects on biological processes related to bone and connective tissue development [3, 4]. In synthetic materials prepared by firing 1 mol SiO_2 with 1 mol hydroxyapatite (HA, Ca/P = 1.67) the resulting silicon stabilized tricalcium phosphate system (Si-TCP) is multiphase with crystalline phase components silicon-alpha-tricalcium phosphate (Si-α-TCP), HA and beta-tricalcium phosphate (β-TCP) and 15–20 wt% of an amorphous phase. Si-TCP has bioactive properties encouraging both osteoclast resorption and osteoblast bone deposition [5, 6]. The multiphase characteristics of Si-TCP arise from the presence of excess SiO_2 which also likely plays a role in the formation of the amorphous component [7]. Si-α-TCP is a single phase form of tricalcium phosphate in which Si is partially substituted for P, and is prepared at lower silicon concentrations by similar chemical and preparation conditions for the formation of Si-TCP except that the ratio Ca/(P + Si) = 1.5 [8]. This follows earlier work by other authors to prepare single phase silicon substituted calcium

hydroxyapatite ($Ca_{10}(PO_4)_{(6-x)}(SiO_4)_x(OH)_{2-x}$) (Si-HA, Ca/(P + Si) = 1.67) [9, 10]. For artificial materials the influence of the impurity on the reaction chemistry of the base material in an aqueous environment is important [11]. Further study and understanding of the hydrolysis of these compounds should provide insight into the material changes which take place in multiphase Si-TCP during in vivo implantation.

Alpha tricalcium phosphate α-$Ca_3(PO_4)_2$ (α-TCP, Ca/P = 1.5) is an important component of cements for biomaterial applications due to its ability to quickly hydrolyze to HA in aqueous media [12, 13]. Mechanisms involved in this hydrolysis process have previously been described [14–17]. Depending on the system conditions, "whisker-shaped" crystallites elongated along the HA c-axis, or plates stunted along the c-axis are often formed. The development of such crystallites was first described by Eanes et al. in 1970 [18] for the formation in solution of hydroxyapatite (HA) from amorphous calcium phosphate (ACP, Ca/P = 1.67). A growth mechanism was proposed: dissolution of the ACP supersaturated the solution and caused apatite particles to grow as diffusion controlled dendritic crystals. Upon completion of the ACP dissolution the apatite particles grow further due to Oswald ripening.

Further insight was given by Christoffersen et al. by phase change and pH studies of compounds resulting from the simultaneous dissolution of $CaCl_2$ and K_2HPO_4 [19]. The calcium to phosphorus ratio of the starting mixture was the same as TCP (atomic ratio, Ca/P = 1.5). At temperatures between 30 and 42 °C, a calcium deficient HA (cd-HA) was produced from intermediate phases including ACP and octacalcium phosphate (OCP). It was shown that an amorphous phase was required to nucleate the cd-HA crystals. Working conditions such as temperature affected the mid and end phases created [20, 21]. At lower temperatures (15 °C), the most thermodynamically stable crystal structure, HA, was not formed and platelets of calcium monohydrogen phosphate dihydrate (DCPD) with a whisker-like crystal morphology appeared.

This paper examines the dissolution and hydration of multiphase silicon stabilized α-TCP (Si-TCP) in Earle's balanced salt solution (EBS), having a composition listed in Table 1, and in water. Since the dissolution processes for all these compounds is slow the process was accelerated through ultrasonic agitation. Of particular interest are the ions appearing in the solution, and the composition, morphology and crystallographic orientation of the crystallites which form. The experimental data shows that the main compound which is formed is HA.

The results are supported by predictions using first principles or *ab initio* computations of the chemical reactivity of different crystal surfaces of hydroxyapatite in water. First principles or so-called *ab initio* methods based on density functional theory and pseudopotentials have been used to simulate bulk and surface properties of calcium phosphates and the effects of Si doping of hydroxyapatite (HA), and tricalcium phosphates (TCP) [22]. When appropriate questions are addressed and great care is taken the methods have predictive capacity and reveal details of the bulk and surface energetics and structure on an atomic scale [23]. The consistency between experiment and theory in the present work demonstrates the potential of such calculations.

Table 1 Composition of Earle's balanced salt solution, EBS Sigma–Aldrich E3024

Ingredients	Composition (g/L)
KCl	0.4
NaCl	6.8
$NaH_2PO_4(\cdot H_2O$	0.122
D-Glucose	1.0
$MgSO_4 \cdot 7H_2O$	0.09767
$CaCl_2 \cdot 2H_2O$	0.265
$NaHCO_3$	2.2

Experimental

Fabrication

Multiphase Si-TCP powders were prepared as described in previous papers [5, 7] An aqueous ammonium phosphate solution was titrated into an aqueous solution of calcium nitrate, adding ammonium hydroxide to keep the pH at 10.5 (0.5, according to the following reaction.

$$5\ Ca(NO_3)_2 + 3\ NH_4H_2PO_4 + 7\ NH_4OH \rightarrow Ca_5(PO_4)_3(OH) + 10\ NH_4NO_3 + 6\ H_2O$$

Silicon was then added to the calcium phosphate precipitate using a colloidal suspension of fumed silica (Cab-o-Sperse™, Cabot Corporation, 500 Commerce Dr. Aurora IL 60504) at a concentration of 1 mol SiO_2:1 mol $Ca_5(PO_4)_3OH$. The resulting calcium phosphate sol was aged at room temperature for 22 h, concentrated by centrifuge, decanted and spray dried in a Yamato-Ohkawara DL-41 spray dryer. The spray dried powders were calcined in open alumina crucibles for 3 h at 200 °C followed by 1 h at 550 °C to remove water and NO_2 associated with the precursor reactants, then sintered for 2 h at 1050 °C. All ramp rates were set at 5 °C/min. All powders were sintered at 1175 °C for 60 min with a ramp rate of 1 °C/min. Powders of pure phase Si-α-TCP, HA, α-TCP and β-TCP were obtained to compare the reactivity of these materials to that of the multiphase Si-TCP.

Hydrolysis

Samples of multiphase Si-TCP powders were ground and sieved (<36 μm) using Retsch sieves. 1 g of powder was immersed in 30 mL of deionised H_2O or Earle's balanced salt solution (Sigma–Aldrich, E3024) respectively for 1, 2, 4, 8, 12, 144 and 720 h, sealed in a glass container and submerged in an ultrasonic bath at room temperature (22 ± 3 °C). A new sterile Earle's balanced salt solution was used at the beginning of each experiment. The pH was verified to be 7.4. Samples of the control powders were treated in the same manner but were immersed for a fixed period of 12 h. Media and powders which were initially mixed uniformly visibly separated within 30 min. Upon completion of the period of immersion in solution, the powders were filtered using Whatman filter paper (<11 μm) and dried in a furnace at 80 °C for 12 h. The filtrate was diluted by a 2 wt% HNO_3 solution in the ratio 1:24 and was elementally analyzed by ion coupled plasma-optical excitation spectroscopy (ICP-OES).

Control powders of pure Si-α-TCP [8], HA (National Institute of Standards and Technology (NIST)), undoped α-TCP (Clarkson Chromatography, Inc.) and β-TCP (Clarkson Chromatography, Inc.) were incubated for 12 h under the conditions described above for the multiphase Si-TCP powders.

Transmission electron microscopy

Transmission electron microscopy (TEM) samples were prepared by lightly regrinding the dried powder and distributing it on a Soquelec copper grid with a Formvar™ substrate. No water or acetone was used during TEM sample preparation to avoid surface modification of the powder.

Two electron microscopes operated in either conventional TEM mode or scanning transmission electron microscopy (STEM) mode were used. Most imaging was done on a Philips CM20 TEM/STEM analytical microscope operated at 200 keV. A ThermoNoran Instruments Energy Dispersive X-ray Spectrometer (EDX) (Model 720B-3SSS) was used simultaneously in STEM mode to collect highly localized elemental fluorescence spectra. The EDX quantification was calibrated using a NIST HA (NIST SRM 2910) standard. Electron diffraction was performed to identify the phases and zone axes using EMS online software [24].

High Resolution TEM (HRTEM) and energy filtered TEM (EFTEM) imaging of the powder samples were performed on a JEOL 2010F TEM/STEM equipped with a field emission gun operated at 200 keV. The amounts of silicon, phosphorus, carbon and calcium present were determined by electron energy loss spectroscopy (EELS) and computed using a three window method of 20 eV bins at energies of 99, 132, 284 and 350 eV respectively over a collection time of 4–10 s depending on the element.

X-ray powder diffraction (XRD)

The phase composition was evaluated by low resolution XRD spectra taken on a Rigaku Mini-flex diffractometer fitted with a copper target. XRD spectra were recorded between 20 and 40° (2θ) in 0.02° steps with 1.2 s counting time per step using the standard $\theta - 2\theta$ Bragg–Brentano geometry. The spectra were compared to standard spectra from the Joint Committee on Powder Diffraction Standards (JCPDS) database [25], including the spectra for α-TCP (JCPDS (9-348), β-TCP (JCPDS (9-169) and HA (JCPDS (9-432), in order to determine the phases present. Phase compositions were estimated from modified Rietveld refinements using Fullprof software [26] for 2θ between 21° and 36° using structural models for HA, α-TCP and β-TCP according to a method described previously [27]. Quality fits for phase quantification were obtained by refining the zero offset, scale factors, and lattice parameters using a pseudo-Voigt peak shape model with predetermined mixing, breadth and asymmetry parameters. Analysis of a matrix of three phase quantitative standard samples indicated that the uncertainty on all phases from every standard was less than 3 wt% (absolute).

Attenuated total internal reflection infrared spectroscopy (ATR-IR)

Total attenuated reflection infrared (ATR-IR) spectra were recorded from 4,000–500 cm^{-1} from powders before and after hydrolysis. Measurements were made on a Nicolet Avatar 320 FTIR Spectrometer with a golden gate single pass diamond ATR accessory. The machine was first calibrated without a sample to compensate for H_2O and CO_2 in the air. Measurements normally signal averaged 32 successive spectra with the time for a complete measurement being about 30s. Powders were sieved to <36 μm to achieve reproducible results. Each spectrum was processed by converting from reflectance to absorbance and then modified with a standard ATR correction which takes into account the dependence of depth penetration on infrared frequency. Further details of these methods are given elsewhere [28].

X-ray photoelectron spectroscopy (XPS)

Low resolution XPS was used to examine the surface elemental composition. Spectra were obtained using a Leybold Max 2090 XPS unit fitted with a dual Al/Mg target. Data was collected using the aluminium anode

operated at 15 kV and 20 mA. Spectra were collected using a pass energy of 192 eV over an analysis area of 4×7 mm^2 at a take-off angle of 90°.

First principles simulation methods

First principles simulations of HA surfaces were performed to assess the relative surface energies and the effect of H_2O adsorption. Electron density functional theory, implemented in the SIESTA software, was used including Troullier–Martins pseudopotentials, Perdew–Burke–Ernzerhof exchange-correlation functionals, Monkhorst-Pack *k*-points and localized orbital basis sets [23, 29–35]. Further details of the computational methods are given in an earlier publication [22] and comprehensive results are presented in [23].

Since the reactions of HA with H_2O are initiated at the interface between the lattice and the medium, surface slab models with periodic boundary conditions were used. These include stoichiometric (001), stoichiometric (010), Ca-rich (010) and PO_4-rich (010), obtained by cleaving the bulk in different ways. The layering which was used to determine the cuts are illustrated in Fig. 1. The cuts were chosen so that the resulting surfaces were charge neutral, and the PO_4 and OH groups remained intact. Note that the (001) surfaces have two possible orientations of OH groups: here we study both and take energies as an average of the two. These planes were chosen to extract basic trends about the effect of water adsorption on crystalline surfaces. Slabs in vacuum and an adsorption of one H_2O molecule per each surface unit cell were considered, and the atomic positions on the surfaces were relaxed to obtain

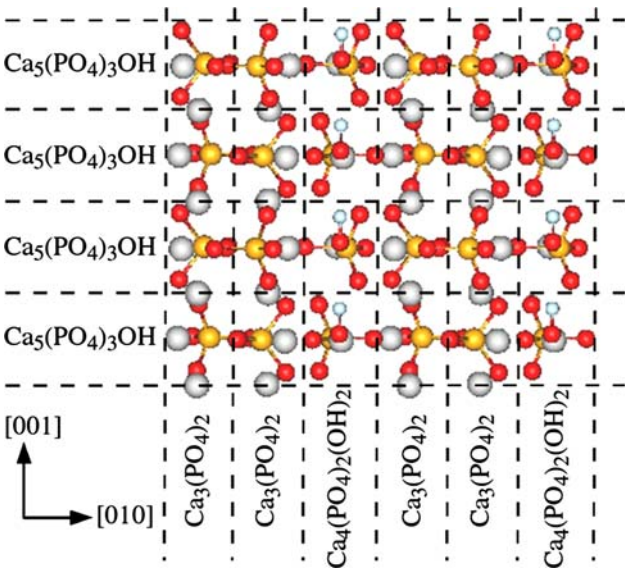

Fig. 1 An atomistic model of stoichiometric $Ca_5(PO_4)_3(OH)$ computed using first principles methods

equilibrium structures. Chemical potential variables are used to compare the energies [36, 37]. Since the stoichiometries of the surfaces differ, the surface energies become functions of the chemical potentials of individual ions μ(xi):

$$S[\mu(x_1),\ldots,\mu(x_n)] = \frac{E_S - E_B + \sum_i^n \mu(x_i)N_i(x_i) - M\mu(H_2O)}{A}$$

N_i is the number of ion species i, A is the surface area, E_S and E_B are the surface slab and bulk energies, respectively, and M, the number of adsorbed water molecules, is either 0 or 1. For the surfaces considered here, the chemical potentials can be simplified into a single variable $\mu[Ca_3(PO_4)_2]$ by imposing a constraint that bulk HA must be in equilibrium with the Ca, PO_4 and OH:

$$\mu(HA) = 10\,\mu(Ca) + 6\,\mu(PO_4) + 2\,\mu(OH).$$

The HA must also be stable against decomposition into other phases, especially $Ca(OH)_2$ and the $\mu[Ca_3(PO_4)_2]$ cannot exceed that of the most stable TCP phase $\mu[\beta$-TCP]. By calculating the total energies of these two phases we obtain upper and lower limits for $\mu[Ca_3(PO_4)_2]$. By assuming zero temperature, the chemical potentials can be replaced by total energies per stoichiometric unit. $\mu(H_2O)$ is taken to be that of a single water molecule.

In addition to H_2O adsorption, exchange processes of the outermost surface Ca^{2+} ions for two H^+ from the environment were studied on the (001) and Ca-rich (010) surfaces. Such a process has been proposed to have a role in HA surface dissolution [38], and its energetics can be studied using the chemical potential approach featured here [23].

Results

Evaluation of the pH with time

In a preliminary experiment, 6.6 g of powder and 200 mL of EBS were mixed in a glass beaker, then let sit in an ultrasonic bath at room temperature. The pH trend reveals a rapid logarithmic increase starting at 7.4 and saturating at ~9. Experiments performed without ultrasonic agitation showed a less rapid increase in pH yet displayed the same trend.

Phase evaluation with time

Changes in the phase composition of the multiphase Si-TCP powder immersed for 1, 2, 4, 8, 12, 144 and 720 h were monitored using XRD, as summarized in Table 2.

Figure 2 compares XRD spectra for the starting powder and for a powder that was immersed for 12 h in EBS. With only an hour incubation the multiphase Si-TCP powder rapidly converts to apatite (>90 wt% HA) in both EBS and H_2O indicating that it is H_2O, and not the ionic composition of the electrolyte that is critical for change. In contrast,

Table 2 Weight percent of phases present in dried powders after different immersion times in EBS and water

Phase composition (wt%)						
Immersion Time (h)	HA	Water Si-α-TCP	β-TCP	HA	EBS Si-α-TCP	β-TCP
0	24 (1)	68 (3)	8 (2)	24 (1)	68 (3)	8 (2)
1	90 (2)	3 (1)	7 (1)	91 (2)	3 (1)	7 (1)
2				93 (3)	3 (1)	4 (1)
4				92 (3)	3 (1)	5 (1)
8				92 (3)	4 (1)	4 (1)
12	93 (2)	3 (1)	4 (1)	90 (3)	4 (2)	6 (1)
144				94 (3)	3 (2)	3 (2)
720	95 (3)	4 (1)	1 (1)	96 (3)	3 (2)	1 (1)

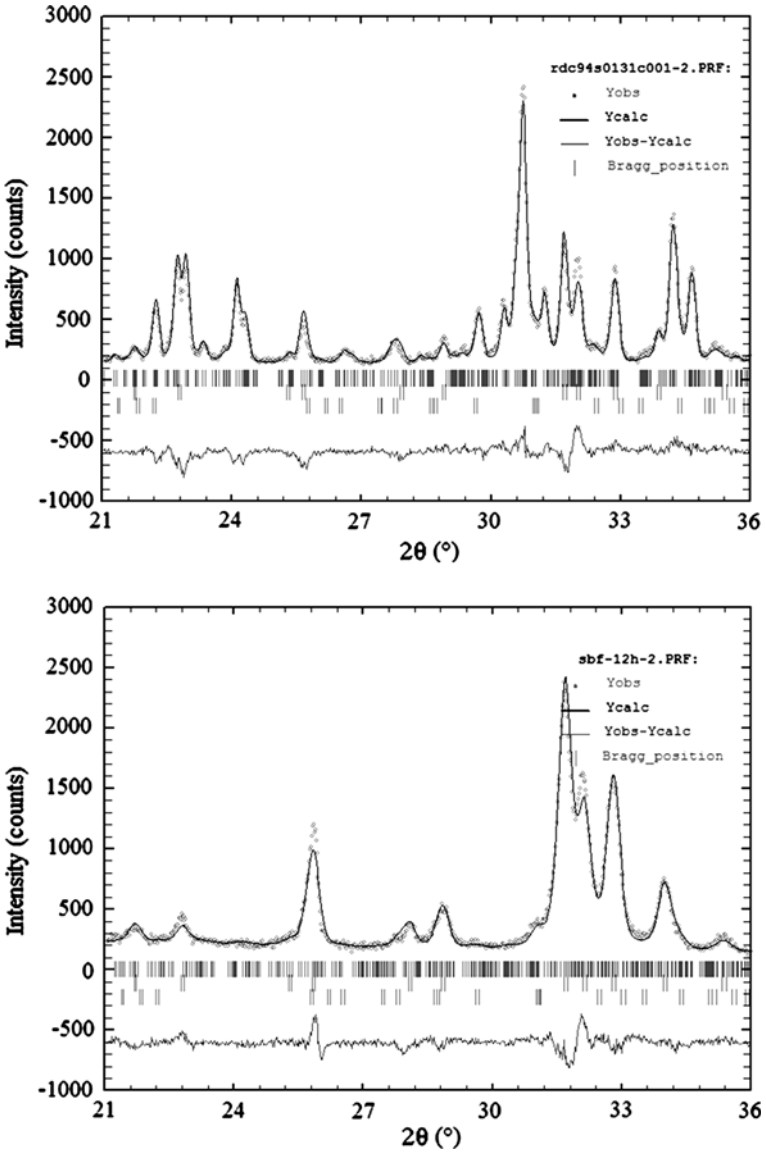

Fig. 2 Rietveld refinements of multiphase Si-TCP powder prior to incubation in aqueous media (top, phase composition is 68(3) wt% Si-α-TCP, 24(1) wt% HA and 8(2) wt% β-TCP) and after ultrasonic stimulation in EBS solution for 12 h (bottom, phase composition is 4(2) wt% Si-α-TCP, 90(3) wt% HA and 6(1) wt% β-TCP)

Table 3 Weight percent of phases present in single-phase powders, as-prepared and after 12 h immersion in EBS. The uncertainties have been modified for correlated residuals [39]

Phase composition (wt%)					
Standard	Immersion time (h)	HA	α-TCP	β-TCP	α-$Ca_2P_2O_7$
NIST SRM 2910 HA	0	99.1 (17)	0.2 (5)	0.7 (4)	-
	12	99.5 (18)	0.3 (5)	0.2 (4)	-
Si-α-TCP	0	0.1 (3)	99.5 (21)	0.4 (5)	-
(0.87 wt% Si)	12	12.7 (6)	86.4 (18)	0.9 (5)	-
Clarkson α-TCP	0	0.1 (9)	87.8 (46)	1.7 (14)	10.4 (22)
	12	0.8 (7)	88.5 (35)	0.1 (10)	10.7 (16)
Clarkson β-TCP	0	0.3 (7)	0.2 (13)	99.5 (45)	-
	12	1.9 (11)	0.5 (16)	97.6 (50)	-

the phase composition of control powders of pure Si-α-TCP, HA, undoped α-TCP and β-TCP show little change after incubation in water or EBS for 12 h, Table 3. Changes in the width of the <002> diffraction peak at 2θ ~25.4° indicates an increase in the crystal size along the c-axis up to 12 h, with a subsequent reduction at 144 and 720 h.

Infrared spectroscopy

Figure 3 compares ATR-IR spectra for the starting multiphase powder with those from powders which had been hydrolyzed in EBS for 1, 12 and 720 h. The major bands around 1017 and 560 cm^{-1} arise from PO_4 vibrations within the apatite structure [7]. These bands are broader for TCP than for the more ordered HA structure. Earlier work on multiphase Si-TCP [28] identified absorption bands at 732 cm^{-1} and 1210 cm^{-1} associated with β-TCP. Bands at 800 and 866 cm^{-1} are associated with Si-O vibrations [40].

The PO_4^{3-} absorption bands narrowed for hydrolysis times of 1 and 12 h in EBS suggesting a transition to an HA structure. OH^- bands in hydroxyapatite [7, 28] are absent at 631 and 3575 cm^{-1} (not shown) even for a hydrolysis times of 720 h, although an increased absorption is noted closer to 650 cm^{-1}. This suggests that the structure of the hydrolyzed crystals differs from that of HA and is more likely that of a non-stoichiometric apatite. After 720 h the ATR-IR spectrum differs little from that for powders hydrolyzed for 1 and 12 h. However, a new doublet arises at ~1400 cm^{-1} which matches the frequencies of carbonate in HA [41]. No carbonate peaks were detected for the same powder in pure distilled deionised H_2O indicating that the carbonate originates from the EBS solution.

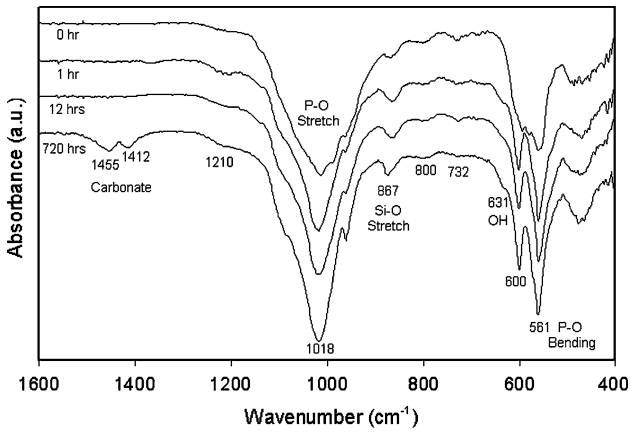

Fig. 3 The ATR-IR spectra (absorbance (%) vs. wavenumber (cm^{-1})) of dried multiphase Si-TCP powder after 0, 1, 12, 720 h in EBS solution—plotted from top to bottom respectively

Electron microscopy

Figure 4a shows the rounded, dense microstructure of a representative particle of the starting multiphase Si-TCP. After hydrolysis, Fig. 4b – the surface was covered by a mass of whisker-like crystallites with individual crystals approximately 100 nm in length and 40 nm in diameter. Figures 5a–c compare the morphology of the starting particle with the surface structure of powder particles which had been hydrolysed for 12 and 720 h. Images of many particles suggested that the dense structure of the original particle had been transformed into a matrix of needle-like crystallites. Imaging of needles was most easily accomplished after 12 h immersion time. At 720 h the needles are smaller with a higher degree of random orientation. It is possible that this results from damage by the ultrasonic agitation. Evaluation of electron diffraction patterns taken from an individual needle showed that the structure had the $P6_3/m$ space group of HA with the needle elongated along the c-axis. These findings are consistent with those reported by Porter et al. [11] in dissolution studies of Si-HA. High resolution TEM of individual needles, Fig. 6, clearly illustrates the lattice planes within the crystallite. The plane spacings are 3.4 ± 0.1Å, which is the spacing between the stoichiometric $Ca_5(PO_4)_3OH$ layers in the <001> direction, as illustrated by the atomistic model of the c-oriented surface shown in Fig. 1.

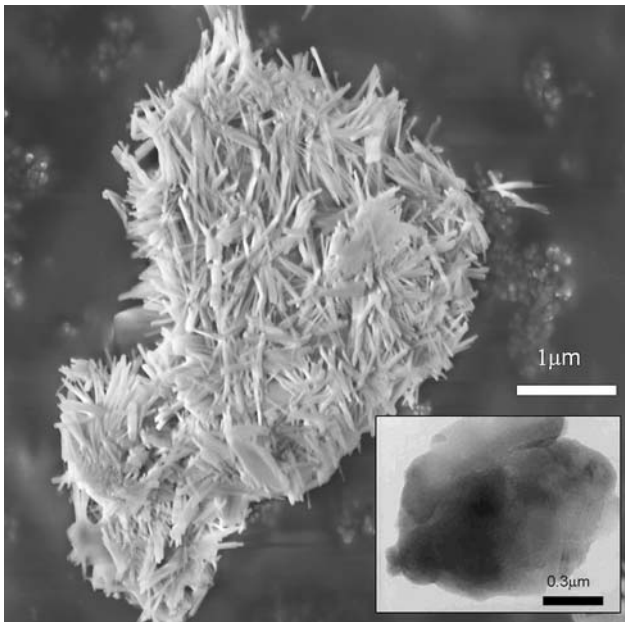

Fig. 4 The surface morphology of a representative particle following hydrolysis in EBS showsneedle-like crystallites that cover the entire surface of the particle. The inset is a representative multiphase Si-TCP particle prior to hydrolysis which has a high density, rounded morphology. The individual particles are not the same

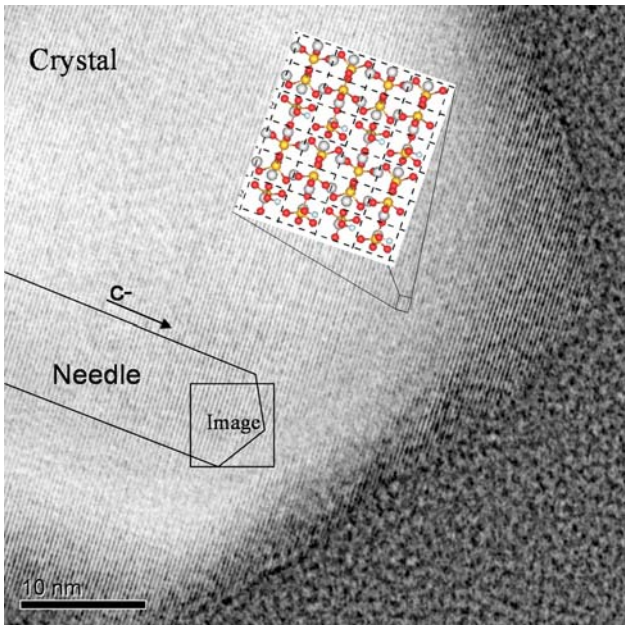

Fig. 6 High resolution TEM shows the end facet of a needle. The plane spacing is 3.4Å, roughly half of the unit cell spacing in the c-direction. Atom colour corresponds to: oxygen is red, calcium is silver and phosphorus is gold

Chemical mapping

Chemical mapping was carried out by energy dispersive X-ray measurements (EDX). An electron beam with a mean spot size of 5 nm was scanned in STEM mode across a particle hydrolyzed in EBS for 12 h and the characteristic fluorescent X-rays were collected. Linescans were used to better resolve low concentrations of Si. The position of the linescan is noted in Fig. 7a and Fig. 7b shows the Ca/P ratio and the Si content as a function of distance. The Ca/P ratio was 1.6 ± 0.5 with strong local concentrations of Si being observed. This corresponds to a small calcium deficiency compared to stoichiometric HA. Figure 8 shows images of individual whisker-like crystallites using energy filtered TEM. Relatively even distributions of calcium and phosphorus were noted throughout the sample. Si was less homogeneous, and in the case shown, high concentrations at the ends of the needles on the (010) surfaces are observed. Significant quantities of carbon, greater than the Si concentration, were detected although it was distributed less homogeneously than Ca and P. Whether this carbon was introduced during preparation, hydrolysis or measurement could not be confirmed for this sample hydrolyzed for 12 h.

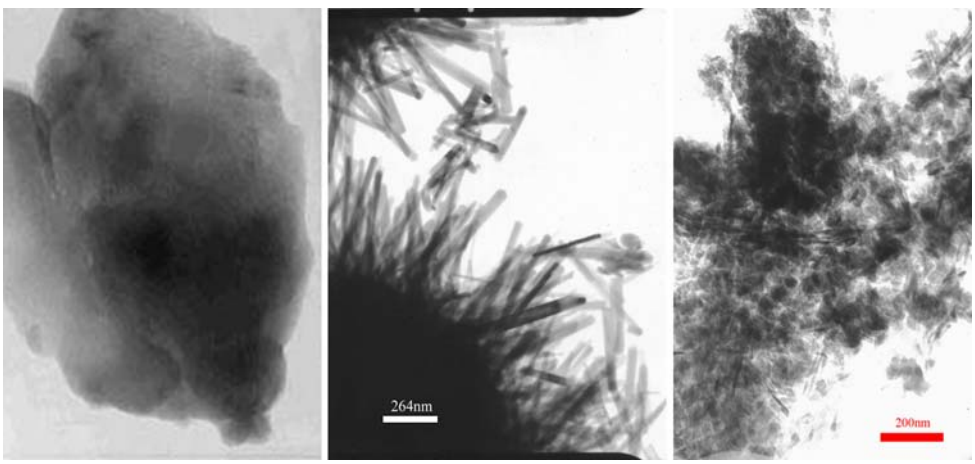

Fig. 5 Images of 1:1 multiphase Si-TCP particle after 0, 12 and 720 h immersion in an ultrasonic bath

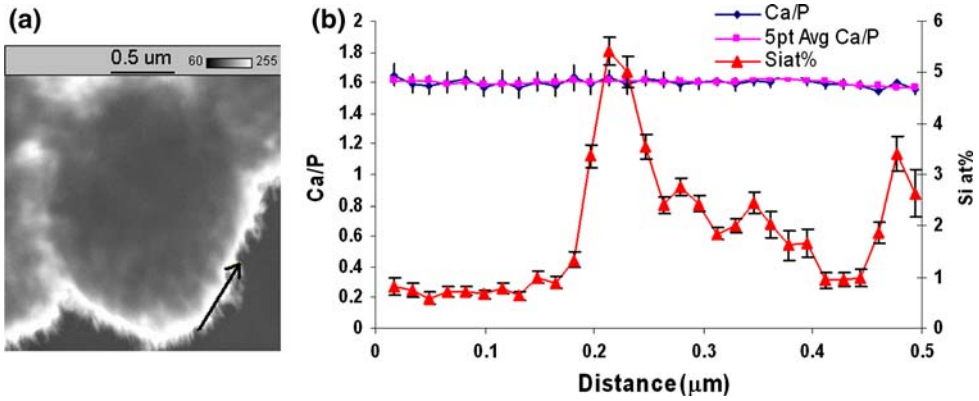

Fig. 7 STEM image (left) and linescan across a sample hydrolysed for 12 h. (**a**) The line on the image indicates the path of the beam. (**b**) Ca/P ratio and Si content as a function of distance along the linescan

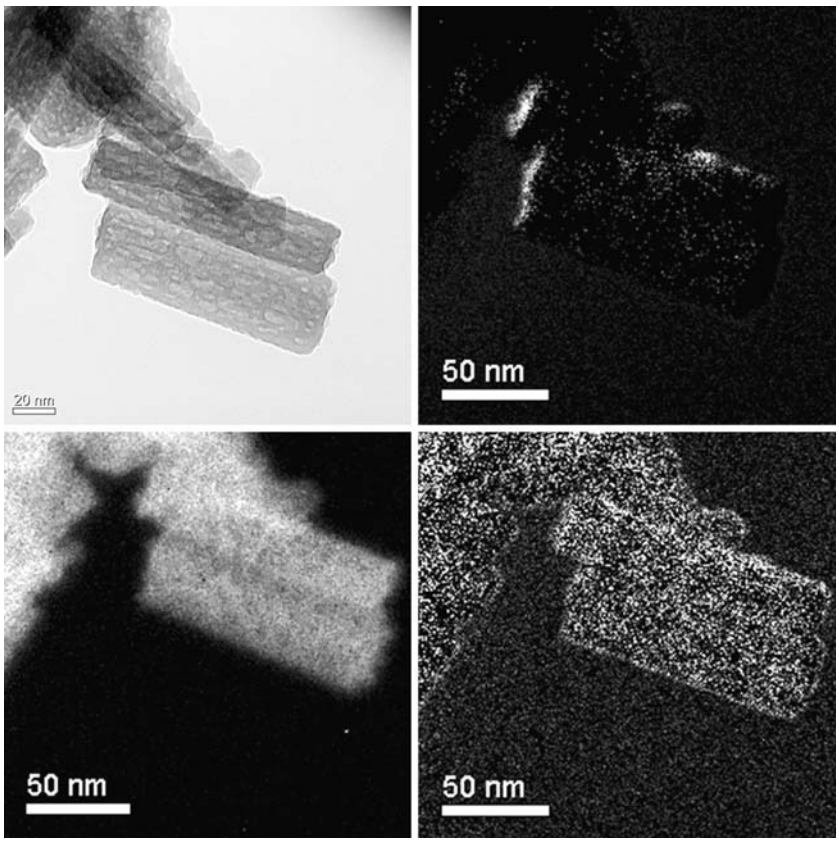

Fig. 8 TEM image of individual needles (top left) and EFTEM images of Si (top, right), P (bottom, left), and carbon (bottom, right)

Media and surface ion exchange

Changes in element concentration in the EBS media in which the powders were immersed are shown in Fig. 9a. The trends for water were similar to that for EBS. Silicon in the medium increased with time, along with a lesser increase of calcium. The phosphorous concentration decreased. This implies that the net Ca/P ratio in the source powder decreases. Although the parameters for the two experiments (mg/L and % change) are not comparable, XPS measurements of the powder surface after drying shown in Fig. 9b indicated a complementary decrease for the concentration of silicon and an increase in phosphorus at the surface. The % change of Ca at the surface also increased and was not complementary to the results for the media. However, the changes in the surface concentration of P and Ca showed similar trends. If even a partial transformation of the surface occurs from TCP (Ca/P = 1.5) to HA (1.67) the expected changes would be $\Delta|Ca|/\Delta|P| = 10/9$. Fig. 9b shows that the measured ratio is smaller than this and that the proposed apatite is calcium deficient. Significant changes occurred in all three element concentrations during the first hour. While this may be simply an effect of the aggressive nature of the ultrasoni-

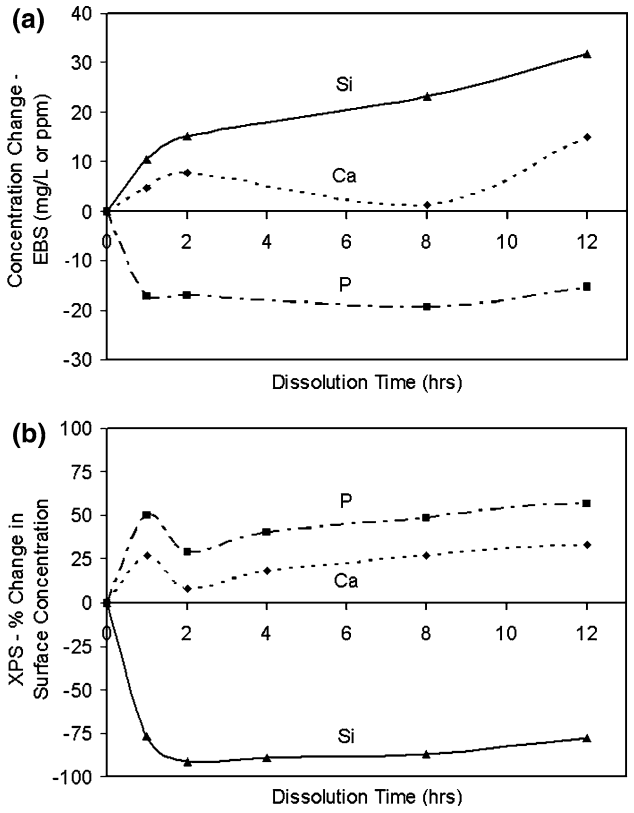

Fig. 9 (**a**) Change in Si, Ca and P concentrations measured by ICP in the EBS media over a 12 h period (mg/L). (**b**) % change in the element concentrations of a dried surface hydrolyzed in EBS and measured by XPS

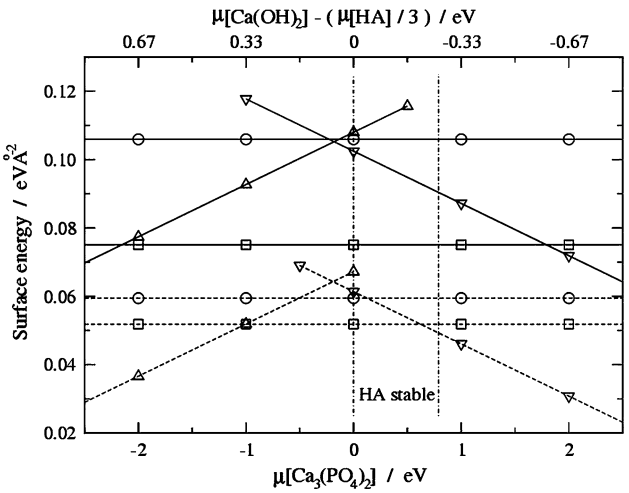

Fig. 10 A comparison of adsorption energies (**a**) for Ca-rich, stoichiometric or PO_4-rich surface slabs in vacuum show that the (001) plane is the most stable in the window of $\mu[Ca_3(PO_4)_2]$ where bulk HA is stable. Solid lines: surfaces in vacuum, dashed lines: surface after single H_2O adsorption, squares: stoichiometric (001), circles: stoichiometric (010), up triangle:PO_4-rich (010), down triangle: Ca-rich (010)

cally enhanced dissolution process, in the multi-phase Si-TCP system in which excess Si is released to the medium, changes in the calcium concentration may be associated with silicon loss.

Discussion

The primary experimental finding is that the multiphase Si-TCP powder transforms rapidly in an ultrasonically stimulated aqueous environment to a needle-like apatite morphology with the c-axis oriented along the needle. Analysis of the EBS and H_2O results after immersion showed that most ion exchange occurred in the first hours of immersion. Infrared studies confirm the transformation with some evidence for ion exchange of species such as carbonate CO_3^{2-}. An interaction must take place between the aqueous media and the original powder which gives rise to a re-crystallization process. This process will occur to minimize the total surface energy and to develop crystallites which have the most stable surface configuration.

First principles calculations of the surface energies of various HA surfaces with and without adsorbed H_2O have been used to model and therefore investigate this process further. Our computations show that the H_2O adsorption energy differs greatly on the different HA surfaces; such differences can influence crystal growth in aqueous environments.

Calculated adsorption energies for different surfaces are compared in Fig. 10. The results for slabs in vacuum show that the (001) layer is the most stable in the window of $\mu[Ca_3(PO_4)_2]$ where bulk HA is stable. However, after H_2O adsorption, the surface energies approach each other, the range where (001) is favorable becomes narrower, and the Ca-rich (010) surface falls into the stability window. This is a result of H_2O being more strongly adsorbed on (010) surfaces. The finding implies that, depending on the ion concentrations in the fluid that determine $\mu[Ca_3(PO_4)_2]$, either Ca-rich (010) or stoichiometric (001) are the dominant faces; the higher the $\mu[Ca_3(PO_4)_2]$, the more elongated in the (001) direction the crystallites would become to minimize the total surface energy. The experimental results are consistent with this prediction.

A characteristic feature of surfaces in vacuum is the presence of under-coordinated O in the surface PO_4 groups. These act as reactive sites for adsorption through the formation of O-H bonds with H_2O leading to a reduction in surface energy. On the stoichiometric (010), dissociative adsorption of water with HPO_4 ion formation was observed. At the (001) surface the O's form a triangle around a Ca ion and are partially coordinated, which accounts for the greater stability in vacuum and smaller adsorption energies for this surface, while on (010) surfaces the O's

Table 4 H_2O adsorption energies on different surfaces of the HA lattice and O-H distances between PO_4 groups and H_2O

Surface	Energy (eV)	d(O-H)	(Ang)
(001)	1.77	1.78	1.86
Stoichiometric (010)	3.04	Dissociated	
Ca-rich (010)	2.69	1.52	1.67
PO_4-rich (010)	2.83	1.64	1.77

bind more strongly to H_2O. This effect is seen when comparing the adsorption energies and O-H bond lengths shown in Table 4. The simulation also found that the loss of a calcium Ca^{2+} compensated by the addition of two H^+ was strongly favored energetically on the (001) and Ca-rich (010) surfaces. This mechanism for Ca loss may be responsible for the measured significant release of Ca into the media. However, it differs from the incongruent dissolution mechanism discussed in an earlier investigation [43], as it applies to the atomistically thin outer surface layer.

The presence of Si in a multiphase system with the predominant crystallographic component being TCP gives rise to a transformation to HA under ultrasonic stimulation which is more rapid than for HA or (-TCP or for single phase Si-TCP. The concentration of Si in the multiphase system is close to 5 wt%, in excess of the 0.87 wt% used to create single phase Si-TCP [7, 8]. A high concentration of Si at grain boundaries in the multiphase material, possibly as a component of the amorphous phase, may allow more rapid chemical attack during hydrolysis, and could be responsible for both the rapid crystallographic transformation and consequent efficient delivery of Si to the surrounding media. Following hydrolysis, the concentration of Si in the media is increased. Given the multiphase nature of the starting Si-TCP powders and the likely presence of an amorphous phase containing Si, it is not possible to conclude from the current results whether Si is incorporated into the transformed apatite to form Si-HA. However, Fig. 8 does show high concentrations of Si on the (010) surfaces of the needles and the ATR-IR data shows an absence of OH^- bands consistent with the incorporation of Si [7, 28]. Future first principles calculations for water adsorption on Si-HA surfaces may be of value to resolve this issue.

Conclusions

A rapid conversion from Si-TCP to a calcium deficient apatite occurs upon contact with aqueous media within hours under ultrasonically stimulated agitation. The crystallite morphology is defined by the minimum total surface energy for adsorption for H_2O and leads to the formation of needle-like crystallites, elongated along the <001> direction. Ultrasonic stimulation accelerates the dissolution and is a useful technique for the study of normally slow dissolution processes, although its immediate effects are not realistic for biological systems. The modification of total surface energy due to H_2O adsorption and the Ca $\rightarrow$ 2H loss mechanism predicted by *ab initio* or first principles calculations suggest that these methods may be of value in predicting chemical and biological parameters.

Acknowledgements Financial support from Millenium Biologix Corporation and the Natural Sciences and Engineering Research Council is acknowledged. The use of ATR-IR was assisted by Dr. Herbert Shurvell of Queen's University. The authors would also like to thank Fred Pearson for operating the TEM at McMaster University, Dr. Greg Cairns, operator of the ICP-OES at the Analytical Services Unit at Queen's University and Dr. Rana Sodhi for XPS measurements at the University of Toronto. Valuable comments and discussions with Dr. Alexis Pietak are appreciated.

References

1. M. BOHNER, *Injury* **31**(4) (2000) 37
2. W. SUCHANEK and M. YOSHIMURA, *J. Mater. Res.* **13** (1998) 94
3. E. M. CARLISLE, *Ciba. Found. Symp.* **121** (1986) 123
4. E. M. CARLISLE, *Sci. Total Environ.* **73** (1988) 95
5. S. D. LANGSTAFF, M. SAYER, T. J. N. SMITH, S. M. PUGH, S. A. M. HESP and W. T. THOMPSON, *Biomaterials*. **20** (1999) 1727
6. S. D. LANGSTAFF, M. SAYER, T. J. N. SMITH and S. M. PUGH, *Biomaterials.* **22** (2001) 135
7. M. SAYER, A. D. STRATILATOV, J. REID, L. C. CALDERIN, M. J. STOTT, X. YIN, M. MACKENZIE, T. J. N. SMITH, J. A. HENDRY and S. D. LANGSTAFF, *Biomaterials* **24** (2003) 369
8. J. W. REID, L. TUCK, M. SAYER, K. FARGO and J. A. HENDRY, *Biomaterials* **27** (2006) 2916
9. S. M. BEST, W. BONFIELD, I. R. GIBSON, L. J. JHA and J. D. SANTOS, "Silicon-substituted Apatites and Process for the Preparation Thereof" (U.S. Pat. No 6312468)
10. I. R. GIBSON, L. J. JHA, J. D.SANTOS, S. M.BEST and W.BONFIELD. in "Bioceramics–Vol. 11", Edited by: R. Z. LEGEROS and J. P. LEGEROS (World Scientific, 1998), p. 105
11. A. PORTER, C. BOTELHO, M. LOPES, J. SANTOS, S. M. BEST and W. BONFIELD, *J. Biomed. Mat. Res.* **69A** (2004) 670
12. K. S. TENHUISEN and P. W. BROWN, *Biomaterials* **19** (1998) 2209
13. L. YUBAO, Z. XINGDONG, and K. DE GROOT, *Biomaterials* **18** (1997) 737 L
14. E. FERNANDEZ, F. GIL, M. GINEBRA, F. DRISSENS, J. PLANELL and S. M. BEST, *J. Mater. Sci. Mater. Med.* **10** (1999) 177
15. M. ANDRES-VERGES, C. FERNANDEZ-GONZALEZ and M. MARTINEZ-GALLEGO, *J. Eur. Ceram. Soc.* **18** (1998) 1245
16. M. P. GINEBRA, E. FERNANDEZ, E. A. P. DE MAEYER, R. M. H. VERBEECK, M. G. BOLTONG, J. GINEBRA, F. C. M. DRIESSENS and J. A. PLANELL, *J. Dent. Res.* **76** (1997) 905
17. M-P. GINEBRA, E. FERNANDEZ, F. C. M. DRIESSENS and J. PLANELL, *J. Amer. Ceram. Soc.* **82** (1999) 2808
18. E. EANES and A. POSNER, *Mat. Res. Bull.* **5** (1970) 377

19. J. CHRISTOFFERSEN, M. CHRISTOFFERSEN, W. KIBALCZYC and F. ANDERSON, *J. Cryst. Growth* **94** (1989) 767
20. C. DURUCAN and P. BROWN, *J. Mater. Sci. Mater. Med*. **11** (2000) 365
21. F. DRIESSENS, M. BOLTONG, E. DE MAEYER, R. VERBEECK and R. WENZ, *J. Mater. Sci. Mater. Med.* **11** (2000) 453
22. R. ASTALA, L. CALDERIN, X. YIN and M. J. STOTT, *Chem. Mater.* **18** (2006) 413
23. R. ASTALA and M. J. STOTT, submitted to J.Chem. Phys. (2006)
24. P. STADELMANN, EMS OnLine, http://cimesg1.epfl.ch/CIOL/ems.html. Last updated August 5, 1998 (Pierre-Henri Jouneau)
25. Joint Committee for Powder Diffraction Studies – International Center for Diffraction Data, and American Society for Testing and Materials, Powder Diffraction File (inorganic and organic), "1601 Park Lane, Swarthmore, PA; 1991)
26. J. RODRIQUEZ-CARVAJAL Fullprof.2k (Version 1.5-Mar2003-LLB JRC) (CEA-CNRS), E-mail: juan@bali.saclay.cea.fr
27. J. W. REID and J. A. HENDRY, *J. Appl. Cryst.* **39** (2006) 536
28. D. DUNFIELD, M. SAYER and H. F. SHURVELL, *J. Chem Phys D* **109** (2005) 19579
29. P. HOHENBERG and W. KOHN, *Phys. Rev.* **136** (1964) B864
30. W. KOHN and C. SHAM, *Phys. Rev.* **140** (1965) A1133
31. P. ORDEJON, E. ARTACHO and J. SOLER, *Phys. Rev. B.* **53** (1996) R10441
32. N. TROULLIER and J. L. MARTINS, *Phys. Rev. B* **43** (1991) 1993
33. J. P. PERDEW, K. BURKE and M. ERNZERHOF, *Phys. Rev. Lett.* **77** (1996) 3865
34. H. J. MONKHORST and J. D. PACK, *Phys. Rev. B* **13** (1974) 5188
35. E. ARTACHO, D. SANCHEZ-PORTAL, P. ORDEJON, A. GARCIA and J. M. SOLER, *Phys. Stat. Sol. (b)* **215** (1999) 809
36. E. KAXIRAS, K. C. PANDEY, Y. BAR-YAM and J. D. JOANNOPOULOS, *Phys. Rev . Lett.* **56** (1986) 2819
37. D. B. LAKS, C. G. VAN DE WALLE, G. F. NEUMARK and S. T. PANDELITES, *Phys. Rev. Lett.* **66** (1991) 648
38. S. V. DOROZHKIN, *J. Colloid Interface Sci.* **191** (1997) 489
39. J. F. BERAR and P. LELANN, *J. Appl. Cryst.* **24** (1991) 1
40. C. HOLLENSTEIN, A. A. HOWLING, C. COURTEILLE, D. MAGNI, S. M. SCHOLZ, G. M. W. KROESEN, N. SIMONS, W. DE ZEEUW and W. SCHWARZENBACH, *J. Phys. D Appl. Phys.* **31** (1998) 74
41. S. KOUTSOPOULOS, *J. Biomed. Mat. Res.* **62** (2002) 600
42. H. M. ROOTARE and R. G. CRAIG, *J. Dent. Res.* **56** (1977) 1437
43. P. W. BROWN and R. J. MARTIN, *J. Phys. Chem. B* **103** (1999) 1671